ELSEVIER

Ultrasonics Sonochemistry 6 (1999) 25–29

Ultrasonics SONOCHEMISTRY

Acoustic cavitation structures and simulations by a particle model

R. Mettin*, S. Luther, C.-D. Ohl, W. Lauterborn

Drittes Physikalisches Institut, Universität Göttingen, Bürgerstraße 42-44, D-37073 Göttingen, Germany

Abstract

Cavitation bubbles in acoustic resonators are observed to arrange in branch-like patterns. We give a brief review of the anatomy of such structures and outline an approach for simulation by individual, moving bubbles. This particle model can reproduce an experimentally observed transition between different structure types in a rectangular resonator cell. © 1999 Elsevier Science B.V. All rights reserved.

Keywords: Bjerknes forces; Bubble dynamics; Cavitation; Particle simulation

PACS: 43.25.Yw; 83.20.Jp

1. Introduction

The emergence of cavitation bubble structures is a common feature of ultrasound applications in liquids. In typical standing-wave resonators with acoustic wavelengths of a few centimeters, the bubble distribution in space is far from being homogeneous. Instead, filamentary branching consisting of moving bubbles that cluster near pressure antinodes is observed (see e.g. [1]). The distribution of bubbles is an important factor for any sonochemical or sonomechanical device where bubbles are involved, and a detailed knowledge of bubble density in space is desirable. The problem of understanding and predicting the cavitation structures is, however, of a quite complex nature. One approach to describe the spatio-temporal evolution of the bubbles is based on suitable averaging procedures to derive a continuous bubble density [2,3]. An alternative approach considers the N-body problem of individual bubbles that move under the influence of the acoustic forces [4,5].

In this paper, we demonstrate the application of the particle approach to cavitation structures that emerge in a rectangular resonator cell. The outline is as follows: Section 2 summarizes some properties of the bubble structures and the experimental setup. In Section 3 we propose the particle model and compare some results to experimental observations. A conclusion is given in Section 4.

* Corresponding author. Fax: +49-551-397720; e-mail: r.mettin@-physik3.gwdg.de.

2. Cavitation structures

An acoustic cavitation structure consists of an inhomogeneous agglomeration of oscillating bubbles of various sizes, moving at different velocities. Fig. 1 shows a snapshot of a typical spatial distribution of bubbles. Because of its similarity to certain electrical discharge patterns we call it an 'Acoustic Lichtenberg Figure'

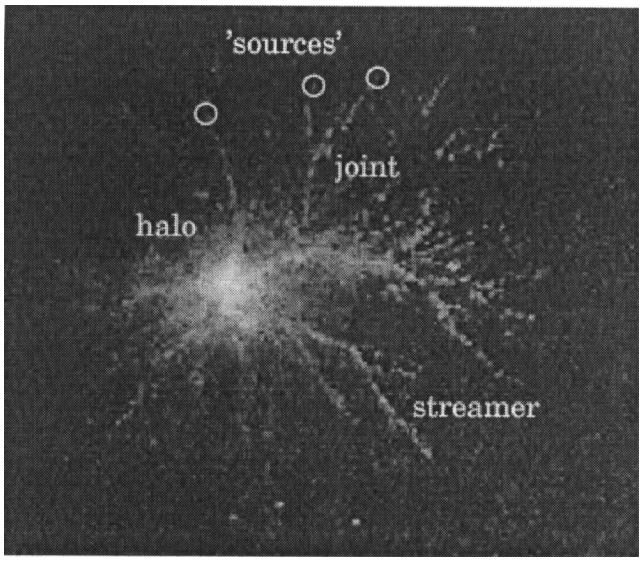

Fig. 1. Acoustic Lichtenberg Figure near a pressure antinode. Some apparent – but not necessarily real – sources of bubbles are encircled, and a streamer, a joint of streamers, and the central halo are labeled. The structure is approximately 3 cm in diameter.

1350-4177/99/$ – see front matter
PII: S1350-4177(98)00025-X

(ALF). Bubbles appear at the outer regions from some 'sources' and migrate inwards to a centre where they accumulate and form a larger cluster. Around the central cluster, a faint mist of microbubbles may be visible as a halo. The bubbles moving towards the cluster form specific paths (streamers), one bubble following the other at a distance of about a millimeter. The paths may unite in joints, thus building an overall filamentary structure. The velocities of the bubbles reach up to about 1 m/s, and the bubble rest radii range from about 10 μm downwards (this value depends on the applied frequency). However, there are still surprisingly few data available in the literature with respect to sizes, velocities and densities of bubbles in cavitation fields.

The bubbles only become visible when they expand during their oscillation to some tens of micrometers. Therefore, the apparent sources of the bubbles do not need to be their true nucleation sites, but only the points of sufficiently large excitation for visibility. Prominent nucleation sites of bubbles are the container walls or impurities in the liquid. Additionally, very small (micro-) bubbles may be carried in streaming liquid and grow slowly by rectified diffusion to a larger size where they start oscillating with large expansion. Microbubbles may be split off from larger oscillating bubbles because of surface instabilities. In particular, the active central cluster, where bubbles continuously merge and disintegrate, serves as a source of microbubbles that form the halo. Invisible outstreaming microbubbles, as well as gas redissolved in the liquid, may provide a way to balance the permanent inflow of bubbles towards the cluster.

The motion of the bubbles (as well as their radial pulsation) is driven by the acoustic field in the resonator. The clustering of the bubbles near pressure antinodes reflects the uneven acoustic pressure distribution in a standing wave field, because the small bubbles involved are pushed towards the antinodes by the primary Bjerknes force [1]. The filamentary structure of an ALF, on the other hand, seems to emerge from an interplay of inhomogeneously distributed (apparent) bubble sources and the secondary Bjerknes force acting between neighbouring oscillating bubbles [6].

In Fig. 2 the experimental arrangement is shown. A cylindrical piezoceramic transducer is glued to the bottom of a rectangular PMMA cell (open on top, base length 5 cm). Tap water is filled to 5 cm height to form a cubic water volume. The (1,1,1) acoustic standing wave mode is excited at a driving frequency $f \approx 20$ kHz. The central pressure amplitude, $\hat{p}_a$, is tunable up to approx. 200 kPa. The following scenario describes roughly what happens for an increase of the driving pressure amplitude: Up to $\hat{p}_a \approx 50$ kPa , no cavitation is perceptible. If the tap water is freshly drawn, the still submersed gas (not cavitation) bubbles are attracted towards the pressure antinode and collide forming a larger bubble [see Fig. 3(a)]. The latter is pushed away from the antinode once it has reached a critical size. At medium high pressure amplitudes, $\hat{p}_a \approx 100$ kPa, streamers appear and an ALF forms near the centre [Fig. 3(c)]. Further increase of the pressure amplitude pronounces the structure. At a certain threshold, however, a transition from one central cluster to many off-centred streamers or clusters is observed: the antinode appears void [Fig. 3(e)]. This regime starts at $\hat{p}_a \approx 150$ kPa and persists for higher amplitudes.

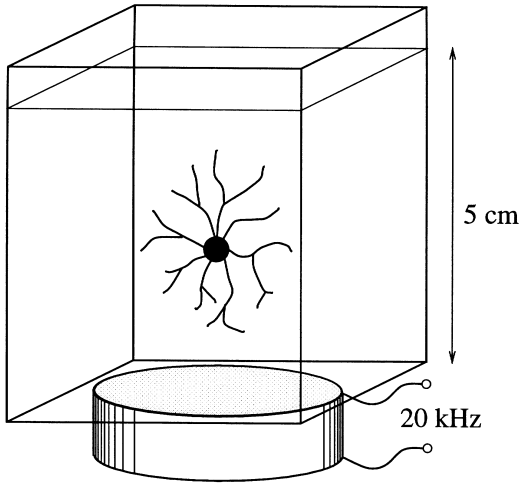

Fig. 2. Cubical resonator cell with the cylindrical piezoceramic transducer glued to the bottom. Cavitation structures like the sketched Acoustic Lichtenberg Figure emerge near the centre for medium high excitation pressure amplitude ($\hat{p}_a \approx 130$ kPa).

3. Particle model simulation

A structure like the one shown in Fig. 3(c) appears to consist of continuous streaks [in sharp contrast to, for example, the slowly moving gas bubbles in Fig. 3(a)]. However, flash light exposure and high speed photography reveal that also the structures caused by cavitation are composed of many single moving bubbles that merely cannot be clearly distinguished by the naked eye or an ordinary video camera. This suggests that a simulation by moving 'particles' might be a suitable tool to capture essential features of the phenomenon. Early steps in this direction have been done by Hinsch [4] who numerically reproduced the motion of a few weakly driven bubbles, oscillating in the linear regime and subject to primary and secondary Bjerknes forces. Our model [5] extends this approach by including nonlinear bubble oscillations. This is important for pressure amplitudes exceeding approximately 50 kPa.

In particular, we determine the motion of N bubbles in the cubic container under consideration of the following forces acting on each bubble: added mass force $\mathbf{F}_M$, primary Bjerknes force $\mathbf{F}_{B1}$, secondary Bjerknes

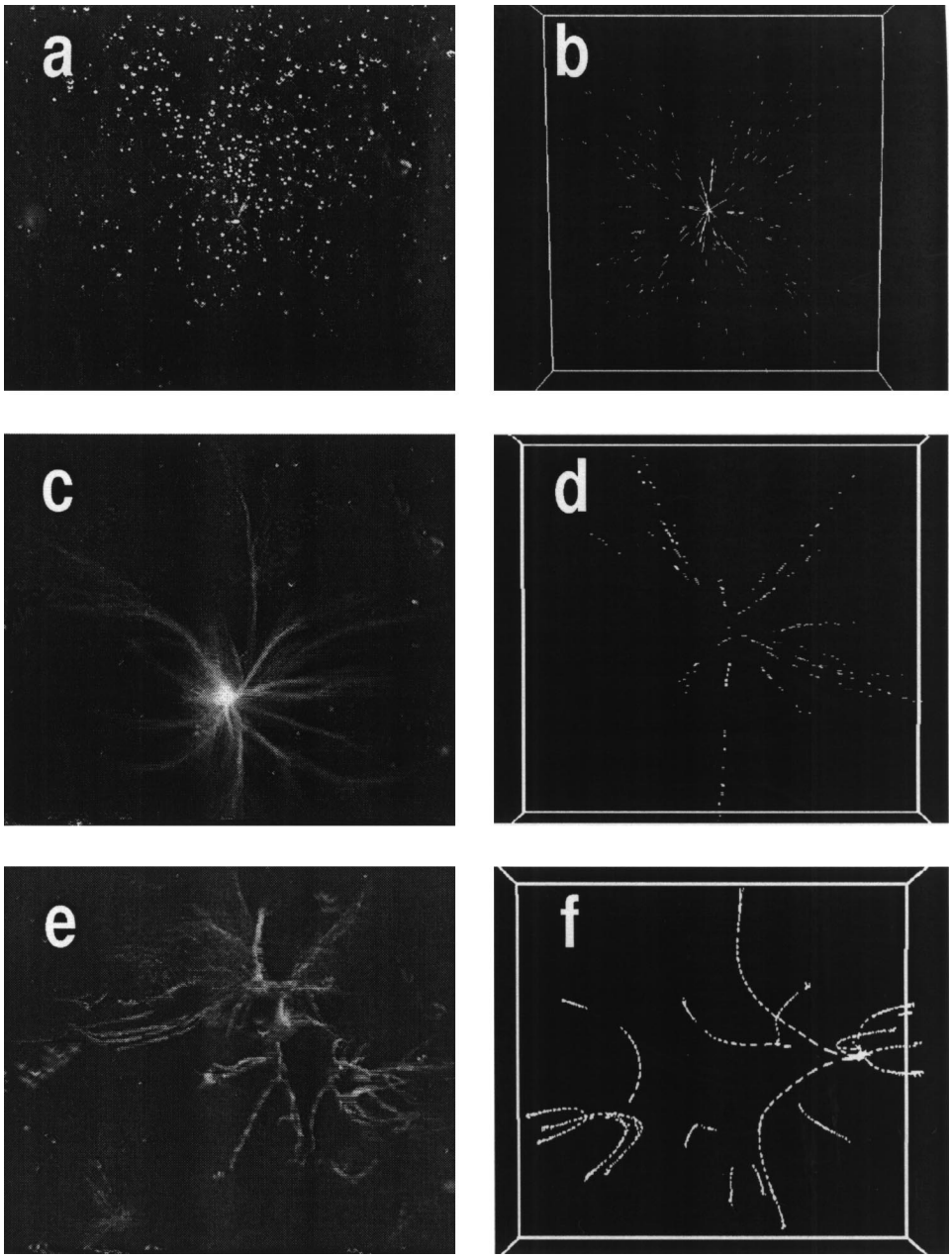

Fig. 3(a). Experimentally observed (left column) and numerically simulated bubble structures (right column). The width of all pictures corresponds to approximately 4 cm. Top row: large submersed gas bubbles move slowly to the centre. (a) Video frame, fresh tap water, $\hat{p}_a \approx 20$ kPa. (b) Snapshot from a simulation with 500 bubbles ($R_0 = 50$ μm) at $\hat{p}_a = 20$ kPa. Middle row: centred cluster of cavitation bubbles (ALF). (c) Video frame, $\hat{p}_a \approx 110$ kPa. (d) 'Long exposure view' of simulation with 200 bubbles ($R_0 = 5$ μm) at $\hat{p}_a = 130$ kPa. Bottom row: off-centred streamers. (e) Video frame, $\hat{p}_a = 130$ kPa. (f) Simulation with 150 bubbles ($R_0 = 5$ μm, $\hat{p}_a = 190$ kPa).

force $\mathbf{F}_{B2}$, and a drag force $\mathbf{F}_D$ (we refer to Refs. [1,7] for the fundamentals). The influence of the bubble density on the exciting sound field is neglected. Further we assume a stationary non-streaming liquid in the cell containing a standing wave $p_a(x;t) = p_a(\boldsymbol{x}) \cos(2\pi f t)$. The model is restricted to spherical bubbles of the same equilibrium size R_0. However, we allow for strongly nonlinear radial bubble oscillations, which is an essential point. The time varying radii $R(t)$ are computed by the Keller–Miksis model, as given in Ref. [8], for the local driving pressure at the bubble's position. We assume slowly moving bubbles, i.e. bubbles do not encounter different sound field amplitudes during one of their radial oscillation period (which is assumed equal to the sound field oscillation period $T = 1/f$ for all bubbles). Then, the forces are determined as follows, involving time averaging over T:

$$\mathbf{F}_M^i = \frac{\rho}{2} \langle V_i(t) \rangle_T \dot{\boldsymbol{v}}_i, \tag{1}$$

$$\mathbf{F}^i_{\mathrm{B1}} = -\langle \nabla p_{\mathrm{a}}(\boldsymbol{x}_i;t) V_i(t)\rangle_{\mathrm{T}}, \tag{2}$$

$$\mathbf{F}^i_{\mathrm{B2}} = \sum_{j\neq i} \frac{\rho}{4\pi}\langle \dot{V}_i(t)\dot{V}_j(t)\rangle_{\mathrm{T}} \frac{\mathbf{d}_{ij}}{|\mathbf{d}_{ij}|^3} \approx f^i_{\mathrm{B2}} \sum_{j\neq i} \frac{\mathbf{d}_{ij}}{|\mathbf{d}_{ij}|^3}, \tag{3}$$

$$f^i_{\mathrm{B2}} = \frac{\rho}{4\pi}\langle \dot{V}_i^2(t)\rangle_{\mathrm{T}}, \tag{4}$$

$$\mathbf{F}^i_{\mathrm{D}} = -[\beta_1 \langle R(t)\rangle_{\mathrm{T}} + \beta_2 \langle R(t)\rangle^2_{\mathrm{T}} |\boldsymbol{v}_i|]\boldsymbol{v}_i. \tag{5}$$

Here, i indexes the bubbles with positions $\mathbf{x}_i$, velocities $\mathbf{v}_i$, and volumes V_i. The liquid density is denoted by ρ, and $\mathbf{d}_{ij} - \mathbf{x}_j - \mathbf{x}_i$ is the vector from bubble i to bubble j. The drag force $\mathbf{F}_{\mathrm{D}}$ is fitted to an experimentally obtained formula proposed by Crum [9] ($\beta_1 = 0.015$ N s/m^2, $\beta_2 = 4000$ N s^2/m^3). The equations of motion $\boldsymbol{F}^i_{\mathrm{M}} = \boldsymbol{F}^i_{\mathrm{B1}} + \boldsymbol{F}^i_{\mathrm{B2}} + \boldsymbol{F}^i_{\mathrm{D}}$ are solved by a semi-implicit Euler method for the N bubbles. To keep the computations simple and fast, we introduced the approximation of equally varying bubble volumes, Eq. (4), for the calculation of the secondary Bjerknes forces $\boldsymbol{F}^i_{\mathrm{B2}}$. This assumes that all neighbour bubbles that contribute significantly to the summation in Eq. (3) feel the same driving pressure amplitude. Additionally, any time delay effects on the bubble interactions are neglected. The time averaged values in Eqs. (1), (2), (4) and (5) are tabulated on a grid in space, and linear interpolation is used for points lying inbetween.

According to the standing pressure wave in the container, the driving amplitude varies in space. Due to this sound field variation, $R(t)$ and the resulting forces can change significantly when a bubble moves to a different position. Fig. 4 illustrates the strong quantitative and

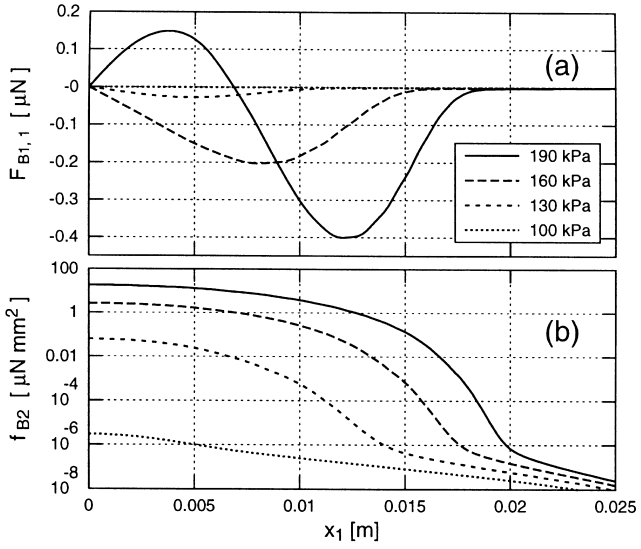

Fig. 4. First component $F_{\mathrm{B1,1}}$ of the primary Bjerknes force (a) and secondary Bjerknes force coefficient f_{B2} (b) vs. the first coordinate x_1 in a cubic resonator (see text; $x_2 = x_3 = 0$ in this picture). The maximum pressure amplitudes $\hat{p}_{\mathrm{a}}$ range from 100 to 190 kPa. Positive values of $F_{\mathrm{B1,1}}$ indicate repulsion from the antinode. Note the logarithmic scaling in (b).

even qualitative variation of the primary and secondary Bjerknes forces for increasing pressure amplitude. The calculations have been done for a cubic resonator (base length $a = 6$ cm, $f = 21.66$ kHz according to the (1,1,1) mode) and a fixed bubble equilibrium size of $R_0 = 5$ μm to come close to the described experiment. The first component of the primary Bjerknes force [$F_{\mathrm{B1,1}}$, Fig. 4(a)] shows increasing attraction (negative values) towards the pressure antinode (the origin) for an increase of driving pressure up to 160 kPa (the negative values associated with 100 kPa, are very close to zero in this scaling). The sign of the force near the origin changes, however, when the amplitude is further increased beyond 170 kPa. As can be seen in Fig. 4(a), at $\hat{p}_a = 190$ kPa the antinode has become strongly repulsive for the bubble size considered. Since the force is still attractive in the outer regions of the standing wave, a stable equilibrium surface forms around the antinode. This is accompanied by an increase of the secondary Bjerknes forces by several orders of magnitude [Fig. 4(b)].

In the model, creation of bubbles takes place near some randomly chosen, but fixed, off-centred sources. This is similar to the experimental observation of bubble occurrence; for short total simulation times, non-moving creation sites seem to be justified. Coalescence is modeled by a certain chance of annihilation after each time step if another bubble is located within a critical distance proportional to $\langle R(t)\rangle_{\mathrm{T}}$. If a bubble vanishes, a new one appears at a creation site. Thus, the total number N of bubbles is kept constant.

The right hand column of Fig. 3 shows typical results from the model to be compared with the experimentally observed structures in the left column. Each picture from the simulations shows overlaid consecutive time steps covering a total time interval Δt, where subsequent positions of each bubble are connected by a straight line. This type of 'long exposure view' is more adequate for a comparison with the video camera frames. The latter have an exposure time of roughly 20 ms, so the artificial exposure times Δt in Fig. 3(b), (d) and (f) are adjusted to approximately this value.

The experimental and simulated bubble patterns look more or less similar. At least, the gross features can be reproduced by the calculated particle motion: At low driving [Fig. 3(b)], the simulated 50 μm bubbles show the slow drift to the centre with only small mutual interaction, just as the large submersed gas bubbles in fresh tap water. The latter additionally rise up because of buoyancy, which has been neglected in the model. For intermediate strong driving pressure, a centred ALF-like structure is produced by the simulation, including joints of streamers [Fig. 3(d)]. Off-centred clustering and more bent bubble paths appear in simulations of high pressure amplitude. This pattern also coincides with the experimental observation, and it apparently

results from two effects: the secondary Bjerknes forces between neighbours become significant at a larger distance from the geometric centre (the pressure antinode), and the antinode itself eventually becomes repulsive for a critical driving amplitude.

In our simulations, not only the resulting structures, but also the respective bubble velocities appear reasonable when compared to the experimental situation. They range up to only a few mm/s in the low driving regime, increase to about 0.1 m/s for the ALF structure, and range up to 0.5 m/s for high excitation pressure.

4. Conclusion

We have given a brief description of cavitation bubble structures and their creation relating to experiment. It was shown that gross features of the structure formation in an acoustic resonator can be captured by a rather simple particle model that takes into account added mass, drag and Bjerknes forces. As an essential ingredient, nonlinear spherical oscillations of the bubbles were used for calculation of the forces. An experimentally observed structure transition between centred and off-centred clustering of bubbles could be reproduced by simulation. Additionally, calculated bubble velocities correspond to experimentally observed values.

An advantage of the proposed model is that the simulation takes place in real scales of time and space, and results of a modeling run can be compared directly with experiment. A very useful, if not indispensable, tool for interpretation of the results is a graphics device that gives a three-dimensional impression of the space–time variation of the structures.

Current restrictions and therefore possible extensions of the particle approach are numerous. For instance, any influence of the bubble distribution on the applied sound field is neglected. Also, a streaming of the liquid is not incorporated. A dispersed bubble size distribution is as well out of the scope of the model as a realistic close interaction, like mergence or disintegration of bubbles. However, the model used here seems to be a good compromise between effort and yield. Moreover, for most of the extensions mentioned above, additional experimental data would be quite helpful. Thus, the exploration of cavitation structures will best proceed by a close connection of theoretical and experimental investigations. As an example, the good correspondence of our simulations to the experiments seems to provide an indirect confirmation of the calculated Bjerknes forces between strongly oscillating small bubbles (compare also [6]).

From a sonochemist's viewpoint, additional questions arise with respect to what might be called the 'active bubble' distribution within a sonoreactor. This would include good predictions of bubble sizes and compression rates of their interior which, in turn, could be related to free radical production rates in the liquid [10]. Up to now, a reasonable link between physical and chemical properties exists only at an incomplete level. The investigation and simulation of cavitation structures as given in this article may be seen as a further step in this direction.

References

[1] T.G. Leighton, The Acoustic Bubble, Academic Press, London, 1994.
[2] Yu.A. Kobolev, L.A. Ostrovsky, J. Acoust. Soc. Am. 85 (1989) 621–629.
[3] I. Akhatov, U. Parlitz, W. Lauterborn, Phys. Rev. E 54 (1996) 4990–5003.
[4] K. Hinsch, The dynamics of bubble fields in acoustic cavitation , in: V.A. Akulichev et al. (Eds.), Proc. 6th Int. Symp. on Nonlinear Acoustics, Moscow University, Moscow, 1975, pp. 26–34.
[5] R. Mettin, C.-D. Ohl, W. Lauterborn, Particle approach to structure formation in acoustic cavitation, in: L.A. Crum et al. (Eds.), Proc. NATO ASI Sonochemistry & Sonoluminescence, Leavenworth, 1997, Kluwer Academic, Amsterdam, 1999.
[6] R. Mettin, I. Akhatov, U. Parlitz, C.-D. Ohl, W. Lauterborn, Phys. Rev. E 56 (1997) 2924–2931.
[7] C.E. Brennen, Cavitation and Bubble Dynamics, Oxford University Press, Oxford, 1995.
[8] U. Parlitz, V. Englisch, C. Scheffczyk, W. Lauterborn, J. Acoust. Soc. Am. 88 (1990) 1061–1077.
[9] L.A. Crum, J. Acoust. Soc. Am. 57 (1975) 1363–1370.
[10] S. Sochard, A.M. Willhelm, H. Delmas, Ultrason. Sonochem. 4 (1997) 77–84.